ISSN (Print) 1226-1750
ISSN (Online) 2233-6656
Journal of Magnetics 24(1), 155-161 (2019) https://doi.org/10.4283/JMAG.2019.24.1.155

Polyindole-Coated Soft-Magnetic Particles and their Viscoelastic Behaviors under Applied Magnetic Field

In Hye Park[1], Seung Hyuk Kwon[1], Hyoung Jin Choi[1]*, Nam Hui Kim[2], and Chun Yeol You[2]

[1]*Department of Polymer Science Engineering, Inha University, Incheon 22212, Korea*
[2]*Daegu Gyeongbuk Institute of Science & Technology, Daegu 42988, Korea*

(Received 14 July 2018, Received in final form 3 December 2018, Accepted 19 December 2018)

To solve the sedimentation drawback of soft-magnetic carbonyl-iron (CI) particles for their application to a magneto-rheological (MR) fluid, the coating of a polyindole (PIn) onto the surfaces of CI microspheres was introduced through chemical oxidization polymerization using 4-aminobenzoic acid as a grafting chemical to increase the interaction between CI particles and PIn. The coated morphology was confirmed using a scanning electron microscope, whereas the reduced density was examined through a gas pycnometer. The effect of the coating on MR performance was analyzed using a rotation rheometer connected with a magnetic field generator. Based on the results of a dynamic oscillation rheological test, the CI/PIn-based MR fluid exhibited a more elastically solid behavior with the applied magnetic fields when compared to a pure CI-based MR suspension, showing an increased magnetic-field strength-dependent storage modulus from a strain sweep test. With a solid-like behavior under an applied external magnetic field, the storage modulus was observed to be higher than the loss modulus within the entire frequency range.

Keywords : polyindole, carbonyl iron, core-shell, magnetorheological

1. Introduction

A magnetorheological (MR) fluid, an actively controllable smart material composed of soft-magnetic particles suspended in a magnetically insulating fluid, forms a solid-like chain arrangement under the applied magnetic field strength. Its fibrillar form is constructed in a direction perpendicular to the magnetic field, and its structure reversibly returns to its original state when the magnetic field is turned off [1]. This phase transition occurs extremely quickly, within milliseconds, and its rheological properties change depending on the morphology of the magnetic particles, surface roughness, magnetic property, dispersing medium, and particle weight fraction [2-7], along with its electrically analogous electrorheological fluid under an applied electric field strength [8]. Thus, MR fluids have been introduced into various industrial areas including the semi-active control of the MR damper, brakes and clutches, polishing devices, and medical applications for drug delivery and cancer therapy [9-12].

Meanwhile, with regard to the usage of magnetic particles, soft-magnetic carbonyl iron (CI) microspheres are extensively adopted materials with excellent magnetic characteristics and an adequate micron-order size [13, 14]. Nonetheless, CI-based MR fluids usually possess a serious dispersion problem induced through a significant density difference between the dispersing medium and the magnetic particles, restricting their use in MR applications of various active control systems when considering the phase variation between fluid- and solid-like materials caused by the input of the magnetic fields. Therefore, using pristine CI particles as a core component of an MR fluid material has two major drawbacks. The first problem is the instability of the particle dispersion owing to the large density of CI particles. The settling occurs quickly, leading to a poor MR effect. Several efforts to improve this problem, including the use of shear thickening fluids [15] or the adoption of a dimorphic MR fluid system [16], have been introduced. As the second problem, bare CI particles might go through an oxidation process when directly exposed to a carrier fluid. Thus, to improve this problem, various CI-polymer core-shell systems

*Corresponding author: Tel: +82-32-860-7486
Fax: +82-32-865-5178, e-mail: hjchoi@inha.ac.kr

This paper was presented at the IcAUMS2018, Jeju, Korea, June 3-7, 2018.

applied to MR fluid particles have been studied. Such polymers include polyaniline (PANI) [17, 18], poly(methyl methacrylate) (PMMA) [19], polystyrene (PS) [20], and poly(glycidyl methacrylate) (PGMA) [21].

Polyindole (PIn) is an emerging conducting polymer owing to its superior thermal stability, redox activity, and slow degradation rate compared to the well-known PANI and polypyrrole (PPy). Indole has an aromatic ring structure linked with a pyrrolitic ring, which is expected to result in the characteristics of both poly(p-phenylene) and PPy [22, 23]. By covering the CI particles with PIn, the shell can prevent the core from being oxidized even at an elevated temperature. In addition, the low density of PIn can lower the density gap between the core-shell magnetic particles and carrier fluid (for example, silicone oil), thereby helping improve the stability of the sedimentation.

In this study, PIn was synthesized using chemical oxidation polymerization as a shell material surrounding the CI core. To increase the affinity among the PIn and CI particles, *para*-aminobenzoic acid (PABA) was adopted as a grafting chemical for inputting a π–π stacking site onto the surfaces of the CI particles [24]. Their core-shell morphology and characteristics were analyzed, and the structural impact on the MR behavior and magnetic property was also investigated.

2. Experiment

2.1. Materials and synthesis

Five grams of spherical CI micro-particles (CC grade, BASF, Germany) were homogeneously suspended in deionized (DI) water (100 mL) while applying ultrasonication. A grafting agent of PABA (1.0 g) (Junsei Chem., Japan) was dissolved in the above magnetic particle-dispersed water mixture and agitated for 3 h under a constant temperature of 5 °C. After modifying the surfaces of the CI particles using PABA, the products were cleaned continuously with DI water to eliminate the unadjusted PABA. Ammonium persulfate (APS) (4 g) (Daejung Chem., Korea), mixed in aqueous hydrochloric acid (0.1 M) (HCl) (Junsei, Japan), was added to a three-neck flask at 15 °C. A monomer solution, prepared by adding indole to a small amount of ethanol, was placed into the reactor dropwise, and the polymerization continued for 12 h to allow the PIn to cover the CI core, as recently reported [25]. Finally, PIn/CI core-shell type microspheres were precipitated using ultracentrifugation, and cleaned with ethyl alcohol, followed by water, to remove the remaining unreacted reagents. The final microspheres were completely dried overnight using a vacuum oven at 65 °C.

2.2. Characterization

The synthesized CI/PIn particles were placed onto carbon tape and their morphology was characterized using a high-resolution scanning electroscope microscope (HR-SEM) (S-4300, Hitachi, Japan). Applying a thermogravimetric analysis (TGA) instrument (Q50, TA Instruments, USA), the thermal properties were determined in a N_2 atmosphere at a heating rate of 10 °C per minute from 25 °C to 800 °C. Their density was measured in a powder form using a gas pycnometer (Accupyc 1330, Micromeritics, USA), whereas the magnetic characteristics were examined using a vibration sample magnetometer (VSM) (Model 7307, Lakeshore, USA). Both pure CI and CI/PIn particles were homogenously mixed in silicone oil (100 cSt) at a sample concentration of 50 wt% to characterize their MR property. The rheological properties were studied using a parallel-plate type rotation rheometer (MCR 300, Anton-Paar, Austria).

3. Results and Discussion

Scheme 1 shows the synthesis route for the coating of PIn onto the micron-sized CI particles. The grafting agent of the PABA adjusts onto the surface of the CI, enhancing the interaction between indole and core. The PIn molecules were synthesized through chemical oxidization polymerization by initiating with the oxidant agent of the APS. The morphology was detected using an SEM, as shown in Fig. 1.

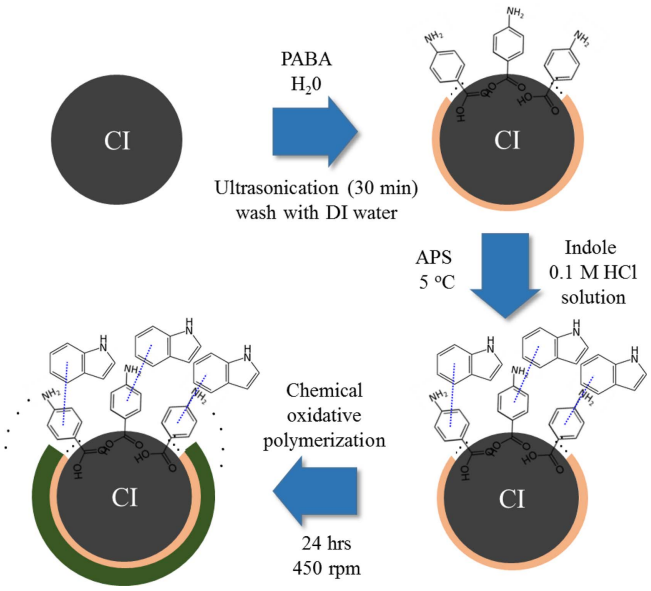

Scheme 1. (Color online) Schematic diagram of fabrication mechanism of core-shell typed CI/PIn microspheres.

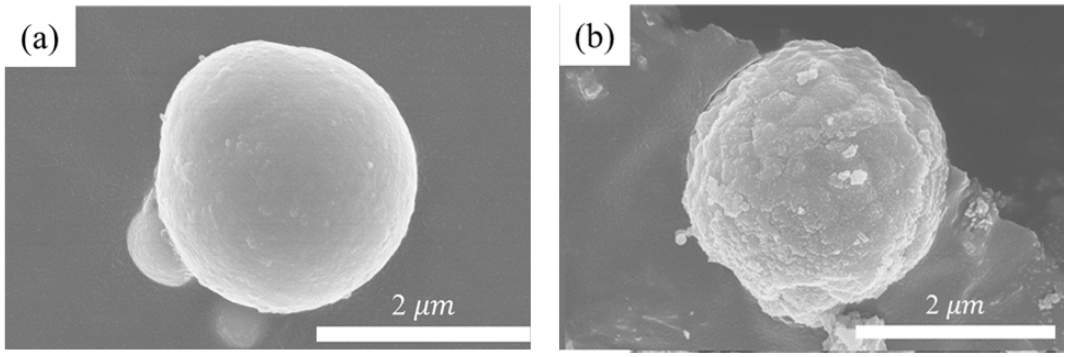

Fig. 1. HR-SEM images of (a) pure CI microsphere and (b) CI/PIn particle.

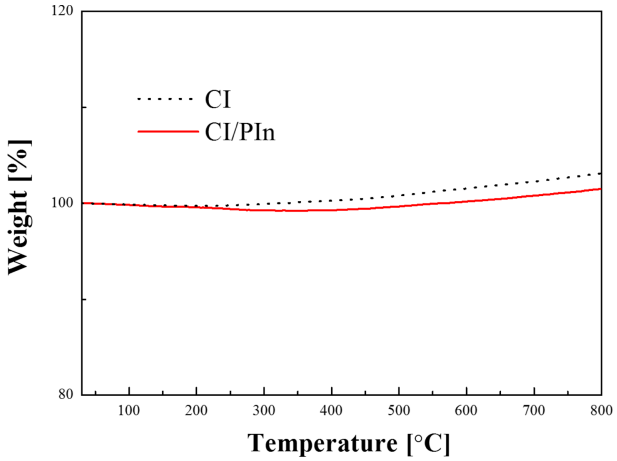

Fig. 2. (Color online) TGA data of CI and CI/PIn microspheres under N_2 atmosphere.

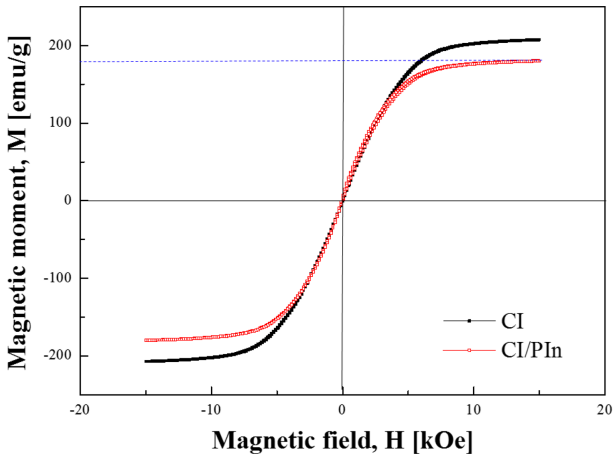

Fig. 3. (Color online) Magnetization loops of CI (closed) and CI/PIn (open) particles in room temperature.

Compared with the neat CI surface in Fig. 1(a), the polymer-coated core-shell CI/PIn particles show a rough surface, as indicated in Fig. 1(b). This clear difference indicates that the polymer coating was successfully applied onto the CI surface.

The thermal stability of the CI/PIn particles was evaluated based on a TGA, as shown in Fig. 2. The TGA curve of the CI particles (dash line) was constant until reaching 200 °C, after which it started to increase slightly. This might have been due to the small amount of oxygen remaining in the TGA equipment. The weight percent of the CI/PIn particles also increased at a similar temperature. However, in the case of the CI/PIn particles, the PIn shell degraded as the temperature increased, showing a decrease in weight percentage of the CI/PIn. The slight decrease in weight percentage indicates how thinly the PIn was coated onto the CI core.

The magnetic properties of both the bare CI and CI/PIn were measured using VSM. The magnetization curve was recorded and plotted, as indicated in Fig. 3, including the saturation magnetization of both types of particles. According to the magnetic hysteresis loop, the saturated magnetizations of the CI and CI/PIn particles were 199.2 and 180.0 emu/g, respectively. The saturated magnetic moment value of the CI/PIn particles was 19.2 emu/g lower than that of the pure CI, which is fully understandable because the nonmagnetic PIn shell decreased the overall magnetic behavior of the CI/PIn composites as compared to the pure CI. Whereas the PIn coating onto the CI particles reduced their magnetic property slightly, owing to the low density of the PIn, the overall density of the CI/PIn composite particles decreased from 7.89 to 7.30 g/cm^3, which was confirmed using a gas pycnometer. The lighter weight of the CI/PIn improved the dispersion stability.

A dynamic oscillation test was conducted under several different magnetic field strengths to investigate the viscoelastic properties of the CI/PIn-based MR suspension as compared to the pristine CI-based MR fluid. Figure 4 shows the strain amplitude sweep measurement for a fixed angular frequency (1 Hz). Both Figs. 4(a) and 4(b) show changes in the dynamic moduli as a function of the applied shear strain. The plateau area of Fig. 4(a) refers to

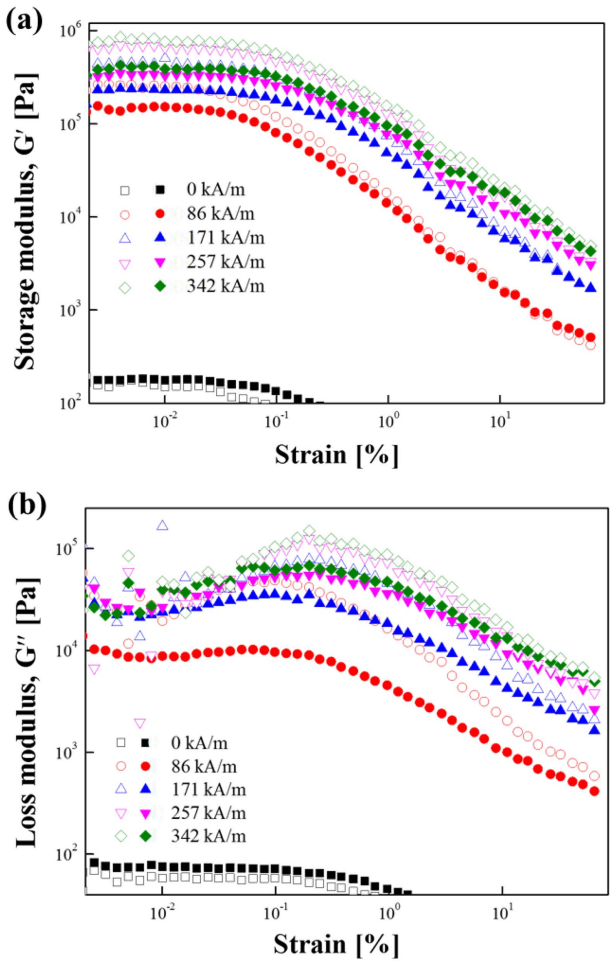

Fig. 4. (Color online) Storage (a) and loss (b) modulus plotted by strain sweep of MR fluids from CI (open) and CI/PIn (closed) particles at a constant frequency 1 Hz.

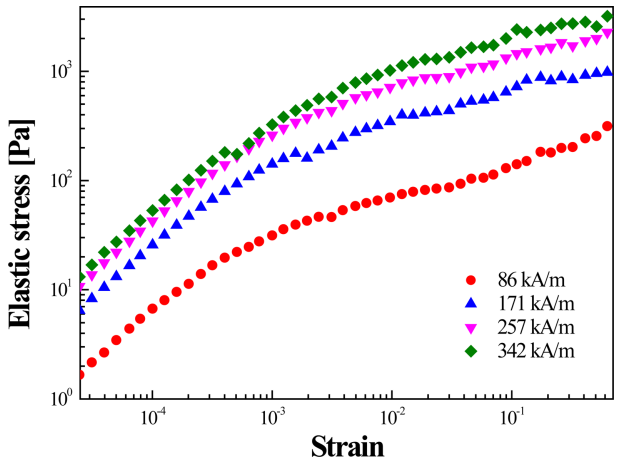

Fig. 5. (Color online) Elastic stresses vs. strain estimated by an amplitude sweep test.

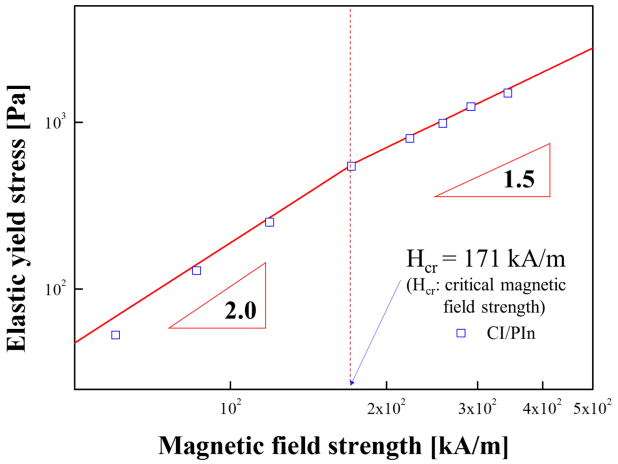

Fig. 6. (Color online) Elastic yield stresses for different magnetic field strength.

a linear viscoelastic (LVE) area, where the value of the storage moduli does not change with an increase in strain. Over this region, the microstructure of the magnetic particle chains formed by the strength of the applied magnetic field remain undisturbed. However, when the strain reaches a critical strain ($\gamma_c = 5 \times 10^{-5}$), the chain structure starts to collapse, which is shown by the decrease in both dynamic moduli.

Based on a strain amplitude sweep measurement, the elastic stress (Fig. 5) under each magnetic field strength was calculated based on Eq. (1).

$$\tau_E = \gamma G'(\gamma) \tag{1}$$

The elastic yield stress at each magnetic field strength, as indicated in Fig. 5, which is the maximum stress at which the broken chains can be completely recovered after stress is applied [1], was estimated and plotted, as shown in Fig. 6.

The yield stresses obtained increase with the development of the external magnetic field strength, the relationship of which differs at a conversion point of approximately 171 kA/m [26]. In detail, the elastic stress below 171 kA/m is proportional to H^2, whereas the elastic stress is proportional to $H^{3/2}$ above such a conversion point. This conversion point indicates the critical magnetic field strength (H_{cr}), and can be expressed through Eq. (2).

$$\tau_y = \alpha H^2 \quad H << H_{cr}$$
$$\tau_y = \alpha \sqrt{H_{cr}} H^{3/2} \quad H >> H_{cr} \tag{2}$$

The reason for this difference in tendency is the local saturation of the particle magnetization [26]. When $H << H_{cr}$, the magnetic polarization is the main force forming the chain structure of the dispersed magnetic particles; however, when H exceeds H_{cr}, the polar regions have already been saturated, leading to a breakdown of

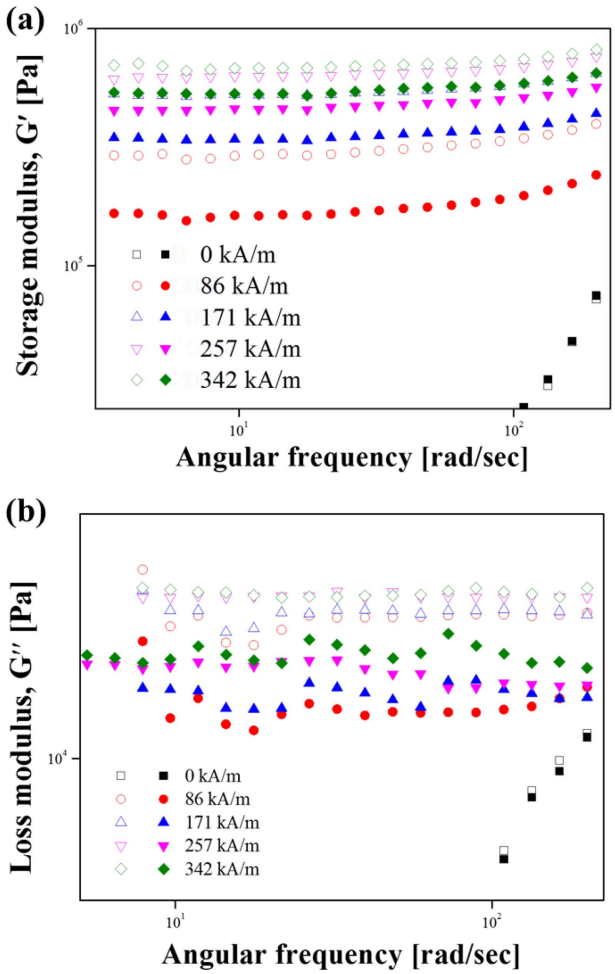

Fig. 7. (Color online) (a) Storage and (b) loss (b) moduli plotted with frequency sweep for CI (open) and CI/PIn (closed) particles based MR fluids in LVE region of constant strain 10^{-4}.

the square dependency [27], which was similarly observed for electrorheological fluids [28].

The frequency relation of both the storage and loss moduli of an MR fluid for a fixed strain of 10^{-4} is plotted in Fig. 7, in which the storage modulus (G') indicates the elastic part of the viscoelastic behavior, and the loss modulus (G'') represent the viscous part. Herein, under an input magnetic field, the values of G' are higher than those of G'' within the entire region of the angular frequency, indicating that the MR suspension demonstrates a viscoelastic solid property owing to the magnetic particle chains. However, without a magnetic field, G' shows a similar behavior as a Newtonian fluid, which is dependent on the increasing angular frequency. The graph also shows the leveling increase in the values of G' and G'' as the magnetic field strength increases, indicating a stronger chain formation [29].

The solid-like property of the formed chain can be

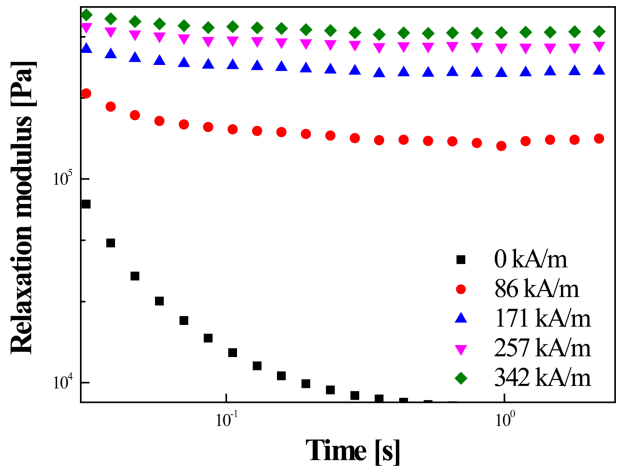

Fig. 8. (Color online) Relaxation moduli $G(t)$ of CI/PIn based MR suspension according to frequency sweep test.

analyzed based on the stress–relaxation behavior, as shown in Fig. 8. The relaxation behavior of the CI/PIn microspheres can be estimated within a short time using the Schwarzl equation [30], which is expressed through Eq. (3).

$$G(t) \cong G'(w) - 0.566G''(w/2) + 0.203G''(w) \qquad (3)$$

Whereas the relaxation modulus decreased with time at a zero magnetic field intensity, it exhibited a plateau behavior under a magnetic field, implying a solid-like chain structure of the CI/PIn-based MR suspension. It was also noticeable that, with an increase in the magnetic field strength, the relaxation modulus also increased owing to the stronger chain structure of the CI/PIn particles [31, 32].

In addition to the plots of $G'(w)$ and $G''(w)$, the loss tangent, namely, the ratio of these two factors, was

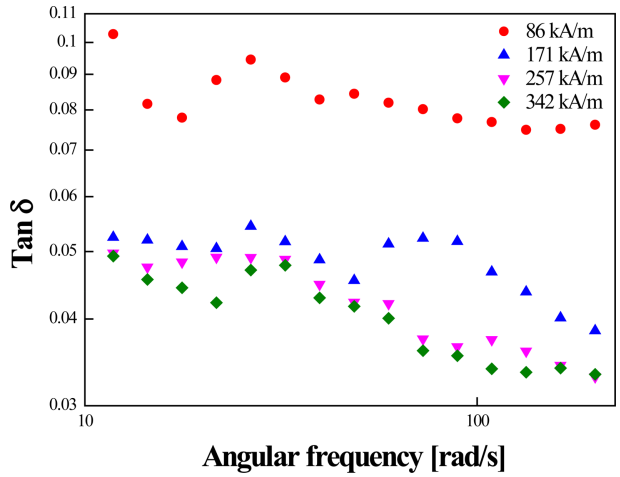

Fig. 9. (Color online) Loss tangent (tanδ) as a fuction of frequency.

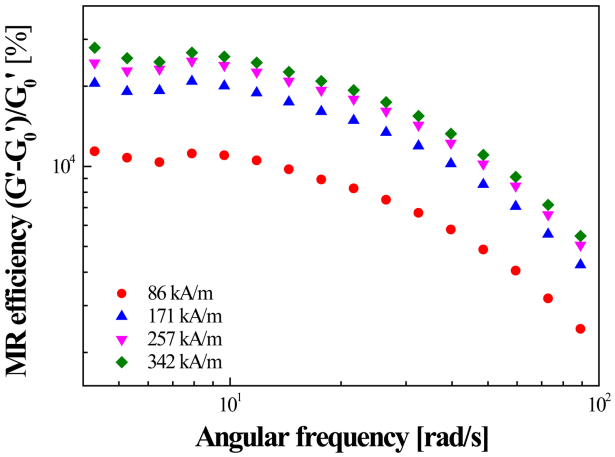

Fig. 10. (Color online) MR efficiency of CI/PIn based MR fluid versus angular frequency in various magnetic field strength.

calculated in terms of the angular frequency, as given in Fig. 9. Note that the loss tangent corresponds to $\tan\delta = G''/G'$, indicating the viscoelastic behavior of the MR fluid. For an ideally elastic behavior with $\delta = 0^o$, $\tan\delta$ becomes zero, whereas for an ideally viscous behavior with $\delta = 90^o$, $\tan\delta$ is equal to 1. Figure 9 shows a viscoelastic solid-like behavior of an MR fluid with CI/PIn. The $\tan\delta$ of the MR sample decreases with an increase in the magnetic field strength, implying a more solid-like behavior. This corresponds with the tendency of the frequency sweep curve [33, 34].

Furthermore, the MR efficiency calculated based on the ratio of the increased storage modulus compared to without the external magnetic field strength is presented in Fig. 10, showing its dependence on the overall angular frequency region. The value of the MR efficiency increases with an increase in the magnetic field strength but decreases within a higher frequency region. This is due to the weakened chain structure of the CI/PIn particles within a higher frequency area, resulting in a weak resistance to the oscillatory rotation [35].

4. Conclusion

A core-shell type CI/PIn composite of soft-magnetic particles was synthesized using the chemical oxidation of PIn at the surfaces of the CI particles using a grafting chemical to enhance the interaction between the magnetic core and PIn shell. All characteristics of the morphology, density, thermal property, and saturation magnetization confirmed the formation of CI/PIn-composite magnetic particles. The MR behavior of the CI/PIn microspheres when suspended in a medium oil was analyzed using a rotation rheometer with a parallel-plate type device under an oscillatory testing method. The elastic yield stresses were observed to be dependent on the magnetic field strengths, with a slope of 2.0 within a low field strength area owing to the magnetic polarization, and a slope of 1.5 once the field strength reached H_{cr}. Typical solid-like characteristics of a CI/PIn microsphere-based MR suspension were also observed from both the dynamic and stress–relaxation moduli.

Acknowledgement

This study was financially supported by Korean National Research Foundation (2018R1A4A1025169).

References

[1] G. Wang, Y. Ma, Y. Tong, and X. Dong, J. Ind. Eng. Chem. **48**, 142 (2017).
[2] I. Arief, R. Sahoo, and P. K. Mukhopadhyay, J. Magn. Magn. Mater. **412**, 194 (2016).
[3] G. Bossis, Y. Grasselli, A. Meunier, and O. Volkova, Appl. Phys. Lett. **109**, 111902 (2016).
[4] I. Bica, E. M. Anitas, and L. Chirigiu, J. Ind. Eng. Chem. **56**, 407 (2017).
[5] T. Plachy, M. Cvek, Z. Kozakova, M. Sedlacik, and R. Moucka, Smart Mater. Struct. **26**, 025026 (2017).
[6] K. J. Son, Korea-Austral. Rheol. J. **30**, 29 (2018).
[7] M. Sedlacik, V. Pavlinek, P. Peerd, and P. Filipd, Dalton Trans. **43**, 6919 (2014).
[8] J. H. Lee, M. S. Cho, H. J. Choi, and M. S. Jhon, Colloid Polym. Sci. **277**, 73 (1999).
[9] S. O. Waheed and N. D. Manring, J. Mech. Des. **140**, 044501 (2018).
[10] A. K. Singh, S. Jha, and P. M. Pandey, Mater. Manuf. Process. **30**, 1482 (2015).
[11] J. Liu, G. A. Flores, and R. Sheng, J. Magn. Magn. Mater. **225**, 209 (2001).
[12] P. Gadekar, V. S. Kanthale, and N. D. Khaire, Int. J. Curr. Eng. Technol. **7**, 32 (2017).
[13] M. Machovsky, M. Mrlik, I. Kuritka, V. Pavlinek, and V. Babayan, RSC Adv. **4**, 996 (2014).
[14] I. Bica, Y. D. Liu, and H. J. Choi, J. Ind. Eng. Chem. **19**, 394 (2013).
[15] X. Zhang, W. Li, and X. Gong, Smart Mater. Struct. **19**, 125012 (2010).
[16] W. Jiang, Y. Zhang, S. Xuan, C. Guo, and X. Gong, J. Magn. Magn. Mater. **323**, 3246 (2011).
[17] T. H. Min, H. J. Choi, N. H. Kim, K. Park, and C. Y. You, Colloids Surf. A **531**, 48 (2017).
[18] M. Sedlačík, V. Pavlínek, P. Sáha, P. Švrčinová, and P. Filip, J. Stejskal, Smart Mater. Struct. **19**, 11 (2010).
[19] J. S. Choi, B. J. Park, M. S. Cho, and H. J. Choi, J. Magn. Magn. Mater. **304**, e374 (2006).

[20] M. A. Lee, F. F. Fang, and H. J. Choi, Phys. Stat. Sol. (a) **204**, 4186 (2007).
[21] M. Cvek, M. Mrlik, M. Ilcikova, T. Plachy, M. Sedlacik, J. Mosnacek, and V. Pavlinek, J. Mater. Chem. C **3**, 4646 (2015).
[22] M. T. Ramesan, Adv. Polym. Tech. **32**, 21362 (2013).
[23] W. Zhou and J. Xu, Polym. Rev. **57**, 248 (2017).
[24] F. F. Fang, Y. D. Liu, H. J. Choi, and Y. Seo, ACS Appl. Mater. Interfaces **3**, 3487 (2011).
[25] I. H. Park and H. J. Choi, J. Ind. Eng. Chem. **64**, 102 (2018).
[26] J. M. Ginder, L. C. Davis, and L. D. Elie, Int. J. Mod. Phys. B **10**, 3293 (1996).
[27] W. H. Chuah, W. L. Zhang, H. J. Choi, and Y. Seo, Macromolecules **48**, 7311 (2015).
[28] T. H. Min and H. J. Choi, Macromol. Res. **25**, 565 (2017).
[29] D. S. Jang, Y. D. Liu, J. H. Kim, and H. J. Choi, Colloid Polym. Sci. **293**, 641 (2015).
[30] I. Emri, B. S. von Bernstorff, R. Cvelbar, and A. Nikonov, J. Non-Newton. Fluid Mech. **129**, 75 (2005).
[31] M. J. Hato, K. Zhang, S. S. Ray, and H. J. Choi, Colloid Polym. Sci. **289**, 1119 (2011).
[32] Y. Seo and H. J. Choi, Korea-Austral. Rheo. J. **30**, 317 (2018).
[33] T. Mitsumata and S. Ohori, Polym. Chem. **2**, 1063 (2011).
[34] B. D. Chin and H. H. Winter, Rheol. Acta **41**, 265 (2002).
[35] C. Y. Gao, M. W. Kim, D. H. Bae, Y. Z. Dong, S. H. Piao, and H. J. Choi, Polymer **125**, 21 (2017).